JGR Oceans

RESEARCH ARTICLE
10.1029/2023JC019953

Alongshore Winds Force Warm Atlantic Water Toward Helheim Glacier in Southeast Greenland

T. Snow[1,2,3], W. Zhang[4], E. Schreiber[5], M. Siegfried[1,6], W. Abdalati[2,3], and T. Scambos[2]

[1]Department of Geophysics, Colorado School of Mines, Golden, CO, USA, [2]Cooperative Institute for Research in Environmental Sciences, University of Colorado, Boulder, CO, USA, [3]Geography Department, University of Colorado Boulder, Boulder, CO, USA, [4]Applied Ocean Physics and Engineering Department, Woods Hole Oceanographic Institution, Woods Hole, MA, USA, [5]UNAVCO, Boulder, CO, USA, [6]Colorado School of Mines, Hydrologic Science and Engineering, Golden, CO, USA

Key Points:

- Alongshore wind-driven coastal upwelling drives Atlantic Water intrusions onto the continental shelf along Sermilik Trough
- This work represents the first remote-sensing evidence of intrusion events along a bathymetric depression
- Rapid intrusions often transport warm subsurface water to the inner shelf and fjord in less than 1 day

Supporting Information:

Supporting Information may be found in the online version of this article.

Correspondence to:

T. Snow,
tsnow@mines.edu

Citation:

Snow, T., Zhang, W., Schreiber, E., Siegfried, M., Abdalati, W., & Scambos, T. (2023). Alongshore winds force warm Atlantic water toward Helheim glacier in southeast Greenland. *Journal of Geophysical Research: Oceans*, *128*, e2023JC019953. https://doi.org/10.1029/2023JC019953

Received 20 APR 2023
Accepted 21 AUG 2023

Author Contributions:

Funding acquisition: M. Siegfried, W. Abdalati, T. Scambos
Methodology: E. Schreiber, T. Scambos
Project Administration: W. Abdalati, T. Scambos
Supervision: W. Abdalati, T. Scambos
Visualization: E. Schreiber, M. Siegfried
Writing – original draft: W. Zhang
Writing – review & editing: W. Zhang, E. Schreiber, M. Siegfried, W. Abdalati, T. Scambos

Abstract Enhanced transport of warm subsurface Atlantic Water (AW) into Greenland fjords has driven glacier mass loss, but the mechanisms transporting AW to the fjords remain poorly characterized. Here, we provide the first direct satellite-based observations of rapid (~0.2 m/s) AW intrusion toward Sermilik Fjord abutting Helheim Glacier, one of Greenland's largest glaciers. The intrusions arise when coastal upwelling—through interactions with Sermilik's bathymetric trough on the continental shelf—triggers enhanced AW upwelling and inflow that can travel tens of kilometers along the trough within hours. A weakening or reversal of northeasterly alongshore winds stimulates the intrusions and is often associated with the passing of cyclones and subsequent sea surface lowering. Mooring data show that these intrusions produce subsurface ocean warming both at Sermilik Fjord mouth and within the fjord and that the warming signal in the fjord does not diminish during subsequent coastal downwelling events. Satellite imagery captures near-synchronous AW intrusions at multiple troughs rimming southeast Greenland suggesting that these wind-driven processes may play a substantial role in ocean heat transport toward the Greenland Ice Sheet.

Plain Language Summary Greater transport of the warm subtropical Atlantic Waters into Greenland fjords has driven glacier mass loss, but the mechanisms transporting the subtropical waters to glacier fronts remain poorly characterized. Here, we provide the first satellite-based observations of rapid flow of subtropical water toward Sermilik Fjord abutting Helheim Glacier, one of Greenland's largest glaciers. Often associated with the passing of cyclones, strong alongshore wind events stimulate ocean circulation that brings subtropical waters from offshore onto the continental shelf along an underwater trough that leads to Helheim. Our measurements show that when these events produce ocean warming nearshore, they tend to transport more heat toward Helheim Glacier's front where it may increase ice melting. A higher number of such wind events in a season has the potential to impact glacier calving, thinning, and retreat. Satellite imagery shows that these events can occur simultaneously along other bathymetric troughs leading toward other Greenland glaciers in the southeast and potentially elsewhere. Therefore, these ocean events may be important for predicting future Greenland Ice Sheet ice loss.

1. Introduction

Helheim Glacier, one of the largest glaciers in Greenland, has experienced multiple dynamic ice loss events over the past two decades (Howat et al., 2005; Williams et al., 2021), as have other neighboring glaciers in southeastern Greenland (e.g., Bjørk et al., 2012; Howat et al., 2008; Luckman et al., 2006; Murray et al., 2010). These regionally synchronous events were likely triggered, at least in part, by enhanced melting at the ice-ocean interface, which has been inferred from glacier observations at many places around Greenland (e.g., Holland et al., 2008; Millan et al., 2018; Mouginot et al., 2015). Acceleration, thinning, and retreat at Helheim Glacier may have corresponded to ocean heating derived from warming or enhanced cross-shelf transport of offshore ocean water into Sermilik Fjord (Figure 1a), the fjord that abuts Helheim Glacier (Murray et al., 2010; Snow et al., 2021). It is unclear, however, what processes modulate ocean heat transport from the open ocean into the fjords and, thus, what may have triggered the past glacier retreat events.

Transport of relatively warm (2.0−5.2°C) Atlantic-origin subsurface waters (AW; found from about 150 to 250 m below surface to the seafloor) delivers much of the ocean heat to Helheim Glacier's front and can vary substantially

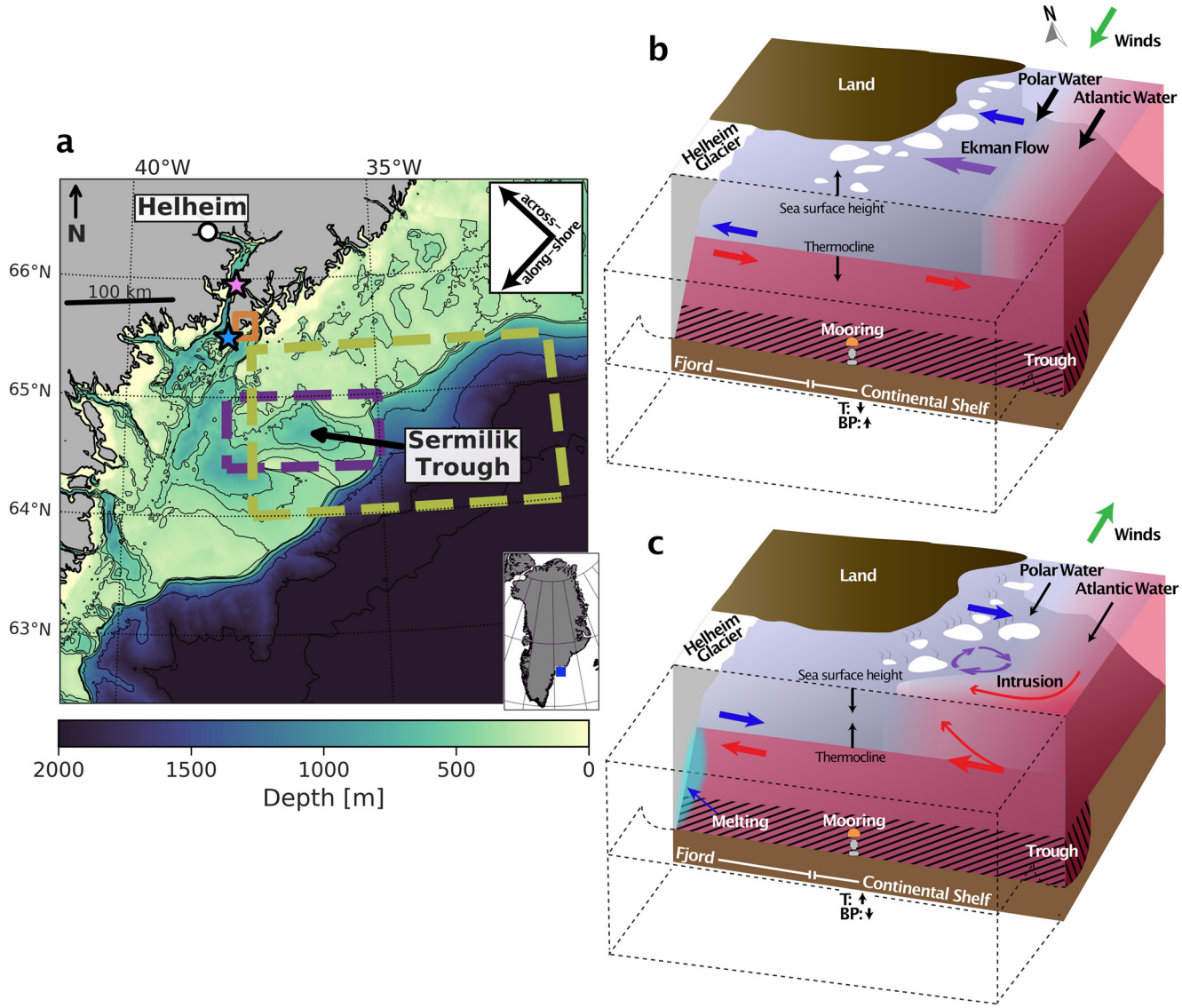

Figure 1. Sermilik Trough study region and wind-driven ocean circulation along the trough. (a) Continental shelf bathymetry near Sermilik Fjord and Trough. Purple, yellow, and orange boxes show the sampling regions for the ERA-5 reanalysis alongshore winds, barrier wind events, and piteraqs (see Section 2), respectively. Stars indicate the continental shelf (blue) and midfjord (pink) mooring locations. Inset shows study location in southeast Greenland. Bathymetry is from BedMachine v3 (Morlighem et al., 2017) with the thin black lines representing contours at 300, 400, 500 m, and every 500 m thereafter. Schematics of the ocean circulation along the axis of Sermilik Trough and Fjord during (b) downwelling-favorable and (c) upwelling-favorable winds. Black arrows indicate current direction and strength within the East Greenland Coastal Current (Polar Water) and Irminger Current (Atlantic Water) on the continental shelf. Red (Atlantic Water) and blue (Polar Water) arrows indicate flow direction in the fjord associated with intermediary circulation, and on the continental shelf from coastal upwelling/downwelling and intrusion along the trough. Clockwise-rotating purple arrows indicate the vorticity created by coastal-trapped waves, which stimulates Atlantic Water intrusion along the trough. White and brown features indicate ice and land, respectively. The presence of a mooring is indicated in the trough with its corresponding observations of bottom pressure (BP) and temperature (T) in each scenario.

due to highly variable ocean circulation patterns between the fjord and the continental shelf (Jackson et al., 2014; Straneo et al., 2010). Within Sermilik Fjord, relatively cold (<4°C) and fresh Polar-origin water (PW) resides at the surface above AW, forming a two-layer circulation structure (Straneo et al., 2010; Sutherland et al., 2014). In summertime, fjord circulation is predominately glacier-melt driven with flow in the surface layer away from the glacier and inflow in the AW layer. However, the dominant variability mode in all other seasons is an oscillatory "intermediary" circulation caused by wind-driven coastal geostrophic currents and changing offshore water-mass properties (Jackson et al., 2014; Straneo et al., 2010; Svendsen & Thompson, 1978). Under this highly dynamic circulation scheme, alongshore northeasterly (prevailing) winds drive onshore surface Ekman transport

(purple arrow in Figure 1b) and create a compensating offshore flow at depth (Håvik & Våge, 2018), resulting in coastal downwelling on the continental shelf (Figure 1b). During such downwelling events (blue and red arrows in Figure 1b), the sea surface height on the continental shelf can rise ∼0.15 m (Cowton et al., 2016; Jackson et al., 2014), isopycnals heave downwards (Jackson et al., 2014; Straneo et al., 2010), and the near-surface PW layer thickens. Opposing southwesterly winds drive the opposite set of changes (Figure 1c). Ocean pressure gradients between the coastal waters and fjord, created by coastal downwelling or upwelling, drive rapid ($\mathcal{O}(hours)$) current reversals within intermediate layers of Sermilik Fjord on synoptic timescales of 4–10 days (Jackson et al., 2014). These strong intermediary currents can flush the upper 300 m of the fjord within days (as opposed to >30 days from melt-driven circulation) and drive large water and heat exchanges between the fjord and continental shelf (Sciascia et al., 2014; Straneo et al., 2010). The wind-driven circulation can either lead to water property variations within the fjord or result in only oscillations with no net water property change (Jackson et al., 2018). It is unclear what conditions drive one outcome or the other.

Outside the fjord, a complex circulation system allows offshore AW below about 300–400 m to intrude onto the continental shelf along a bathymetric trough (∼15 km wide, ∼400–900 m deep) in an onshore flow of $\mathcal{O}(1)$ Rossby number that leads to Sermilik Fjord and Helheim Glacier (Figure 1a; Harden et al., 2014; Snow et al., 2021; Sutherland et al., 2013). On the continental shelf, the East Greenland Coastal Current (EGCC; nearest shore) and East Greenland Current (EGC; further offshore) flow at the surface along the coast carrying PW equatorward (Sutherland & Pickart, 2008), and AW spreads onto the shelf beneath them. Offshore from the continental break, the Irminger Current (IC) carries AW southward throughout the upper water column (Johannessen et al., 2011; Rudels et al., 2002; Våge et al., 2011), which can be diverted onto the shelf (Harden et al., 2014; Snow et al., 2021; Sutherland et al., 2013). Aside from general inflow at depth, full-depth AW inflow occurs on synoptic timescales (2 days to 2 weeks; hereafter referred to as "rapid") along the trough or as seasonally varying (long timescale) inflow across portions of the continental shelf. Intrusions of AW may be linked with EGCC/EGC variability (Harden et al., 2014; Murray et al., 2010; Sutherland et al., 2013), cyclonic eddies (Bruce, 1995; Sutherland et al., 2013; Sutherland & Pickart, 2008), tidal variability, or fluctuations in alongshore winds (Hampson, 2020; Harden et al., 2014) that stimulate coastal-trapped waves (CTWs) (Fraser et al., 2018) coherent for hundreds of kilometers along the shelf (Gelderloos et al., 2021). However, little work has been done in the Sermilik continental shelf region to link the open ocean and fjord during these events, so the drivers of the intrusions and linkages to water property changes nearshore remain unclear.

Rapid intrusions of offshore waters onto continental shelves have been observed and modeled to occur along bathymetric valleys, canyons, and troughs around the globe (Cottier et al., 2005; Fraser & Inall, 2018; Kämpf, 2006; Lentz et al., 2014; Nilsen et al., 2008). Field observations at some locations (e.g., Hudson Shelf Valley, West Spitsbergen Shelf) have demonstrated that coastal upwelling can induce full-water-column intrusions from offshore onto the continental shelf with velocities of >0.2 m/s (Cottier et al., 2007; Inall et al., 2015; Lentz et al., 2014). The flow speed of these intrusions varies regionally as a result of ocean stratification, Coriolis forcing, wind stress, and other regional differences (e.g., Nilsen et al., 2008; Ramos-Musalem & Allen, 2019). Numerical models suggest these inflows result from onshore pressure gradients (often wind-driven) (Kämpf, 2006; Klinck, 1996; She & Klinck, 2000) and are associated with CTWs generated at the bathymetric depression (e.g., Allen & Madron, 2009; Johnson, 1978; Kämpf, 2012; Killworth, 1978; Zhang & Lentz, 2017). The flow responses to along-shelf winds of opposite directions are asymmetric (i.e., strong offshore flow does not occur during coastal downwelling) (Inall et al., 2015; Lentz et al., 2014; Zhang & Lentz, 2017), and strong stratification can restrict the vertical extent of the onshore flow to the deeper portions of the water column (Ramos-Musalem & Allen, 2019). Observations of these intrusions are sparse, and most hydrographic and mooring measurements lack the combined spatial (horizontal or vertical) and temporal coverage required to contextualize the events. They have also never been observed on the Greenland continental shelf. Previous work in Sermilik Fjord (Jackson et al., 2014, 2018; Straneo et al., 2010) and along Greenland's southeastern coast (Harden et al., 2014; Le Bras et al., 2018; Oltmanns et al., 2014; Sutherland & Pickart, 2008) has shown strong correlations between ocean circulation patterns and various wind drivers, including cyclones, barrier winds (high wind speed flow parallel to the coast), and piteraqs (hurricane-intensity downslope winds in the offshore direction); these relationships support the notion that winds may drive intrusions along continental shelf troughs in this region.

Here, we show the first remotely sensed evidence of rapid intrusions of offshore water along the Sermilik Trough leading to Sermilik Fjord. Temperature contrast between warm offshore AW and cold coastal PW make detection of the intrusion by remote-sensing feasible. We use MODerate Resolution Imaging Spectroradiometer (MODIS)

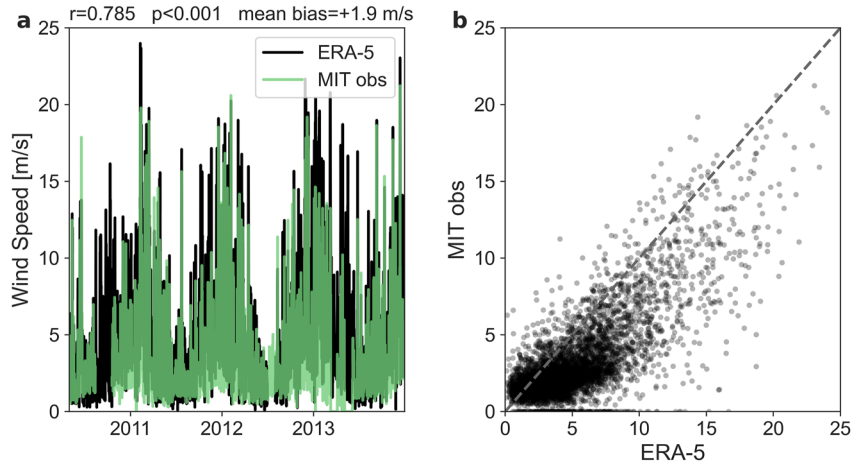

Figure 2. Comparison of ERA-5 (black) near-surface wind speeds with ground measurements made by the Program for Monitoring of the Greenland Ice Sheet (PROMICE) MIT weather station (green) from 2010 to 2013 as a (a) time series and (b) scatterplot. The dashed line in (b) represents a one-to-one agreement. Pearson's *r* represents the correlation between time series with seasonal signal and trends removed.

sea surface temperatures (SST) and optical imagery of the area to characterize AW intrusions and infer their effect on the water column based on observed patterns. Unlike previous work on AW variability within Sermilik Fjord and near the fjord mouth, we provide a continental shelf-wide view of the AW intrusion and its variability from 2010 to 2013 with coincident ocean mooring observations. We show that coastal upwelling, often associated with upwelling-favorable winds generated by the passing of a cyclone and subsequent sea surface lowering, likely drives these intrusions and brings warm water into Sermilik Fjord at depth. This work demonstrates that remote sensing and reanalysis data provide an accessible approach for studying these wind-ocean features in the Greenland coastal region where their impact on glacier mass loss may be important, but in situ ocean observations are rare or nonexistent.

2. Data and Methods

2.1. Satellite Imagery

We initially identified AW intrusion events along Sermilik Trough using MODIS optical imagery from NASA WorldView (MOD02HKM/MYD02HKM Terra/Aqua Level 1B Calibrated Radiances, 500 m resolution; MODIS Characterization Support Team, 2017) to characterize these intrusions and determine their frequency and variability in time (Table S1 and Figure 2). The key observable in MODIS imagery that indicated an intrusion event was the ice-free ocean surface cross-cutting the EGCC toward shore along the Sermilik Trough. To ensure we consider ocean features solely associated with these along-trough intrusions, we identified the most distinctive (i.e., most obviously ice-free ocean surface) AW intrusion events and selected intrusions that were clearly associated with the circulation path leading from the continental shelf break to Sermilik Fjord and either:

1. Travel inshore along the Sermilik Trough between 38.2°W and 37.2°W to at least 65.3°N (inner extent of the trough), or
2. Cut more than 15 km inshore at ~65°N (outer extent of the trough) from the sea ice edge along the trough when the EGCC was wide and covered most of the continental shelf.

Less distinctive sea ice-free waters that do not clearly cut across the EGCC may be attributable to other ocean processes (e.g., eddies traveling south along the continental slope) and do not necessarily indicate intrusions of AW. They are not counted in our analysis. We considered clusters of intrusions that have fewer than 3 days of separation to be one event. We analyzed the satellite observations during 2010–2013 when simultaneous moored temperature records existed for the area and only for January through June when EGCC sea ice cover makes the intrusions readily identifiable. We use MODIS SSTs from the Group for High Resolution Sea Surface Temperature (GHRSST) Level 2P Global Sea Surface Skin Temperature v2019.0 products from the NASA Aqua and Terra satellite (JPL/OBPG/RSMAS, 2020a, 2020b; Kilpatrick et al., 2015) to determine the surface ocean

temperature during the intrusions. The GHRSST products provide SSTs that have already been masked for cloud and ice.

2.2. Atmospheric Conditions

We investigated atmospheric variability influences on the intrusion events using atmospheric reanalysis data from the ECMWF ERA-5 operational reanalysis data (Copernicus Climate Change Service, 2017; Hersbach et al., 2018). The mean sea level pressure (Harden et al., 2011) and large-scale wind field over the Greenland Ice Sheet (not expected to resolve fjord-scale variability; Moore et al., 2015; Oltmanns et al., 2014) and ocean near Sermilik Fjord (Harden et al., 2011; Oltmanns et al., 2014) have been shown to be well-captured by ERA-Interim (previous version to ERA-5) reanalysis data in the region, though ERA-Interim underestimates peak wind speeds by ∼1–2 m/s over the ocean. Ground-based wind speed measurements captured by the Program for Monitoring of the Greenland Ice Sheet (PROMICE) MIT weather station (65.6922°N, 37.82.80°W) are also well-represented by the 10 m wind speeds from ERA-5 (mean bias: +1.9 m/s; Pearson's r: 0.785, p: <0.001; Figure 2). Therefore, similar to ERA-Interim, we assumed the large-scale wind field surrounding Sermilik Fjord remains well-captured in the more recent data product.

We used ERA-5 6 hourly 10 m wind fields, instantaneous turbulent surface stresses, and mean sea level pressure fields (0.5° × 0.5° grid) to determine atmospheric changes before and after the intrusions. The northeasterly alongshore wind velocity and stress are defined as the component of each parameter along the principal axis of the shelf: 242° from north. We recognize that the shoreline and trough bends near the Sermilik Fjord region and a slightly more north/south wind direction may be more suitable for determining alongshore upwelling/downwelling. However, these values provide similar results, so we use 242° to be consistent with previous work (e.g., Straneo et al., 2010). We averaged ERA-5 wind speed and stress over a region of Sermilik Trough we defined as between 64.4°N and 65.0°N, 38.0°W and 35.0°W (Figure 1a, purple box), which represents an area where winds have the strongest correlation with regional EGCC transport changes and the greatest impact on trough transport (Harden et al., 2014; Le Bras et al., 2018). We then rotated the wind velocity and stress vectors to determine the northeasterly alongshore wind components. An alongshore northeasterly wind component (positive) represents coastal downwelling-favorable winds; a southwesterly wind (negative) represents upwelling.

We derived cyclone frequency and tracks using a cyclone detection and tracking algorithm (Crawford et al., 2020; Crawford & Serreze, 2016). To identify barrier wind events, we averaged winds across the southern Denmark Strait region (64.0°N to 65.4°N, 37.5°W to 31.5°W; yellow box in Figure 1a). Any events with >20 m/s winds between 0° and 90° (clockwise) were identified as barrier wind events following (Harden et al., 2011). Piteraqs (or downslope wind events) were similarly identified from winds averaged across the Tasiilaq region (65.5°N to 65.7°N, 37.82°W to 37.42°W; orange box in Figure 1a) if wind speeds reached >10 m/s from between 270° and 20° (clockwise) following (Oltmanns et al., 2014). Similarly to the intrusion events, we considered barrier wind events or piteraqs that occurred in rapid (i.e., fewer than 3 days) succession to be one event.

2.3. Ocean Observations

We investigated the extent to which intrusions affect ocean properties nearshore and within Sermilik Fjord by examining ocean temperature and sea surface height (SSH) during the intrusion events. We analyzed temperature data within the Sermilik Trough and Fjord (Figure 1a) collected by moorings deployed between 24 August 2009 and 18 August 2013 (Harden et al., 2014; Jackson et al., 2014; Jackson & Straneo, 2016). For the continental shelf mooring (Figure 1a, blue star), we used the temperatures from either a Microcat SBE37SM or XR 420 RBR sensor deployed between 262 and 301 m depth near the mouth of Sermilik Fjord. We also used SSH records from (Harden et al., 2014), which were calculated using bottom pressure measurements at the same shelf mooring. The fjord mooring (Figure 1a, pink star) was located midfjord (32 km from the shelf mooring; ∼70 km from Helheim Glacier's front) and had sensors deployed between 120 and 131, 250 and 294, 324 and 350, and 390 and 400 m depths (referred to as the 125 m, 250 m, 350 m, and 400 m records, respectively). Midfjord mooring temperatures were recorded using similar instruments as the continental shelf mooring (Jackson et al., 2014) at 7.5–15 min intervals and were averaged to 6-hourly observations. These moorings provide a time varying record of subsurface AW flowing onto the continental shelf and into Sermilik Fjord (Jackson & Straneo, 2016; Straneo et al., 2011).

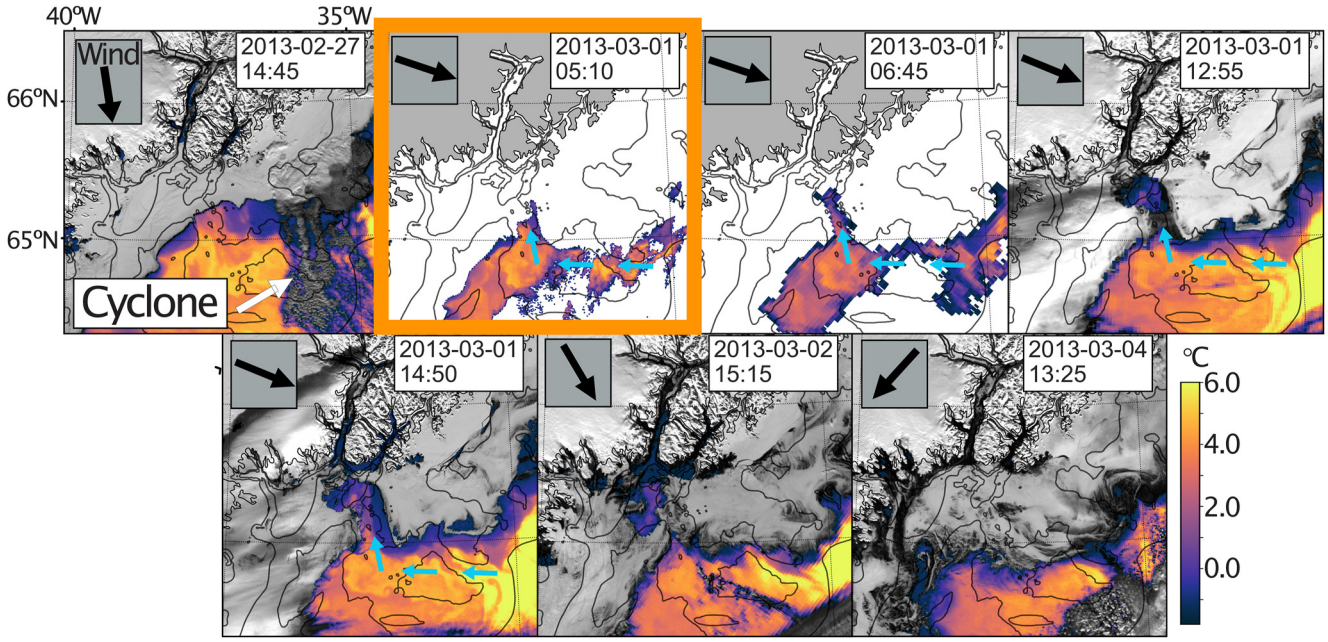

Figure 3. Evolution of an example Atlantic Water (AW) intrusion event near Sermilik Fjord. Selected MODerate Resolution Imaging Spectroradiometer (MODIS) optical imagery during an AW intrusion event from 27 February 2013 to 4 March 2013 overlain with MODIS-derived sea surface temperatures (SST); black arrow indicates wind stress direction averaged over Sermilik Trough. The cyclone (white arrow) was identified separately as a low in ECMWF mean sea level pressure that corresponds to the swirling cloud cover apparent in regional MODIS imagery. Optical imagery is not available for the 05:10 and 06:45 passes on 1 March 2013, as both of these scenes were before sunrise; gray indicates land instead for these images. SSTs not shown in areas with sea ice or cloud cover. The orange box highlights the intrusion initiation after the shifting of alongshore wind stress over Sermilik Trough. Dark gray contours indicate the 250 and 500 m isobaths, which outline the location of Sermilik Trough. Blue arrows indicate the right-hand side of the trough and the AW intrusion path.

As fresher currents running along the shelf, the EGCC and EGC may moderate the AW intrusion events by serving as a barrier (Murray et al., 2010) or diluting the intruding waters as they cross the continental shelf (Snow et al., 2021). Presumably, this influence of the EGCC/EGC changes with their width. To investigate this possibility, we estimated the monthly aggregated width of the surface PW layer during intrusion events using MODIS SST-derived observations of PW extent following (Snow et al., 2021). The analysis is based on the MODIS Level 3 SST V2014 products (Minnett et al., 2019). We sampled MODIS SSTs from the same trough region as (Snow et al., 2021) (13 14 km × 14 km sampling boxes), calculated the SST anomaly relative to the Irminger Current temperature, and then generated a monthly mean for each sampling box. We approximated the PW width along the trough by measuring the distance from the fjord mouth (65.6°N, 38.0°W) to the center of the last sampling box along the trough transect that had a SST anomaly <-1.5°C, a previously defined threshold for delineating temperature difference between surface PW within the EGCC and AW from the IC (Snow et al., 2021). The EGC is difficult to distinguish from the EGCC based on temperature and we cannot be sure we are capturing the EGC using our temperature threshold. Therefore, we refer to the width of the PW layer nearshore herein as the "EGCC width" and recognize it may also include the EGC.

3. Results

3.1. Intrusion Event Characteristics

AW intrusions are observable throughout the MODIS record near Sermilik Fjord, and their size and extent appear to vary widely. A rapid AW intrusion near Sermilik Fjord from 27 February 2013 to 4 March 2013 serves to illustrate characteristics of the bathymetrically steered onshore intrusion and demonstrate the types of observations required to assess them (Figures 3 and 4). The intrusion bisected the sea ice covered EGCC, making the intrusion observable with optical imagery. Prior to the intrusion, sea ice hugged the coast and flowed southward under persistent prevailing northeasterly winds (a 17-day pattern recorded by ECMWF reanalysis; not shown). On 27 and 28 February, cloud cover obscured the surface, but wind shifted to westerly at ∼10 m/s late on 27 February 2013 and again on 1 March after the passing of two cyclones (second cyclone shown in Figure 4). A

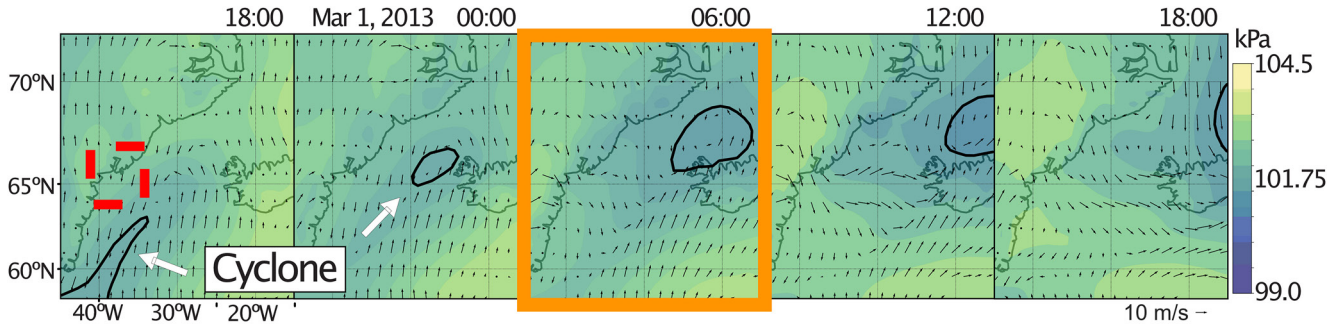

Figure 4. Mean sea level pressure snapshots overlain by wind speed vectors from 18:00 on 28 February 2013 to 18:00 on 1 March 2013. The red box outlines the location of the Sermilik Trough and Fjord. Orange box highlights the time of the shifting of alongshore wind stress over Sermilik Trough and the intrusion initiation. Thick black contour indicates the cyclone.

MODIS sea surface temperature (SST) image from 1 March 2013 (05:10 UTC) showed a warm water intrusion had started (Figure 3, Movie S1). A subsequent image (12:55 UTC) showed the front of the intrusion flow had moved >40 km across the EGCC, bringing AW from the offshore IC almost to the mouth of Sermilik Fjord along the northeastern flank of the Sermilik Trough. Portions of the AW intrusion were ~3.7°C warmer at the surface than surrounding EGCC and fjord waters. Differences between a sequence of 2 March 2013 images shows surface outflow from Sermilik Fjord and the remnants of the intrusion being encroached upon by sea ice within the EGCC, both moving south with the current. By 4 March 2013 when winds returned to their prevailing northerly direction, the cross-shelf intrusion was no longer visible on the surface and no evidence of an opposing offshore flow occurred. This phenomenon has not been previously observed using remote sensing, and its influence has not been accounted for in regional ocean models. Intrusions of this kind will rapidly advect AW and heat into Sermilik Fjord, toward Helheim Glacier, increasing the likelihood of melting (Figure 1c), and therefore serving as an important factor in glacier dynamics.

We visually identified 58 intrusion events during winter and spring (January to June) between 2010 and 2013 (Figure 5 and Table S1). All intrusions are marked by ice-free, relatively warm waters (in comparison to the surrounding sea ice covered EGCC and fjord surfaces) cutting through sea ice along Sermilik Trough, which we interpret as surface AW inflows. In several of the farthest traveling intrusions, cross-shelf velocities were between 0.13 and 0.19 m/s based on the distance that the intrusions crossed within a 24 hr period. Within 24–48 hr after the intrusion became visible in optical imagery, sea ice and cool surface water (observed in SST) spread outward from the coast except along the trough between sequential images (Figure 3 and Movie S1). The cold, ice-free surface water that expands outward from Sermilik Fjord mouth along shore to the south (1 March 2013 14:50 and 2 March 2013 15:15 panels in Figure 3) indicates surface outflow from the fjord during intermediary circulation. Based on the distance that the ice-free water edge moves between images, the surface outflows have approximate velocities of 0.35–0.7 m/s near the fjord mouth, which are consistent with fjord surface velocities measured by Jackson et al. (2014) during intermediary circulation.

3.2. Wind and SSH Conditions Before Intrusion Events

Intrusions coincided most frequently with cyclones and barrier wind events, but not piteraqs unless the piteraqs were also accompanied by the other wind events. Intrusions most frequently occurred after the passing of a cyclone (67% of selected intrusions) or similar low-pressure system offshore (26%) and less frequently with only a high pressure system over Greenland or the Irminger Sea (i.e., blocking event; 7%). We observed six barrier wind events (or clusters of events) between January and June across the 4 years. These barrier wind events accompanied the strongest northeasterly (i.e., downwelling-favorable) winds across our records and all preceded AW intrusion events (Figure 5). We observed 15 piteraqs, seven of which coincided with AW intrusion events (12% of the total intrusion events), and all but one of the seven were associated with simultaneous westerly to southwesterly (i.e., upwelling-favorable) winds offshore.

Local alongshore wind velocity and SSH shifts preceded the AW intrusion events (Figure 5). Winds during most of the intrusion events took two forms within the 24 hr preceding the intrusions: (a) winds that shifted from the prevailing northeasterly direction to a westerly direction, and (b) winds that weakened following strong

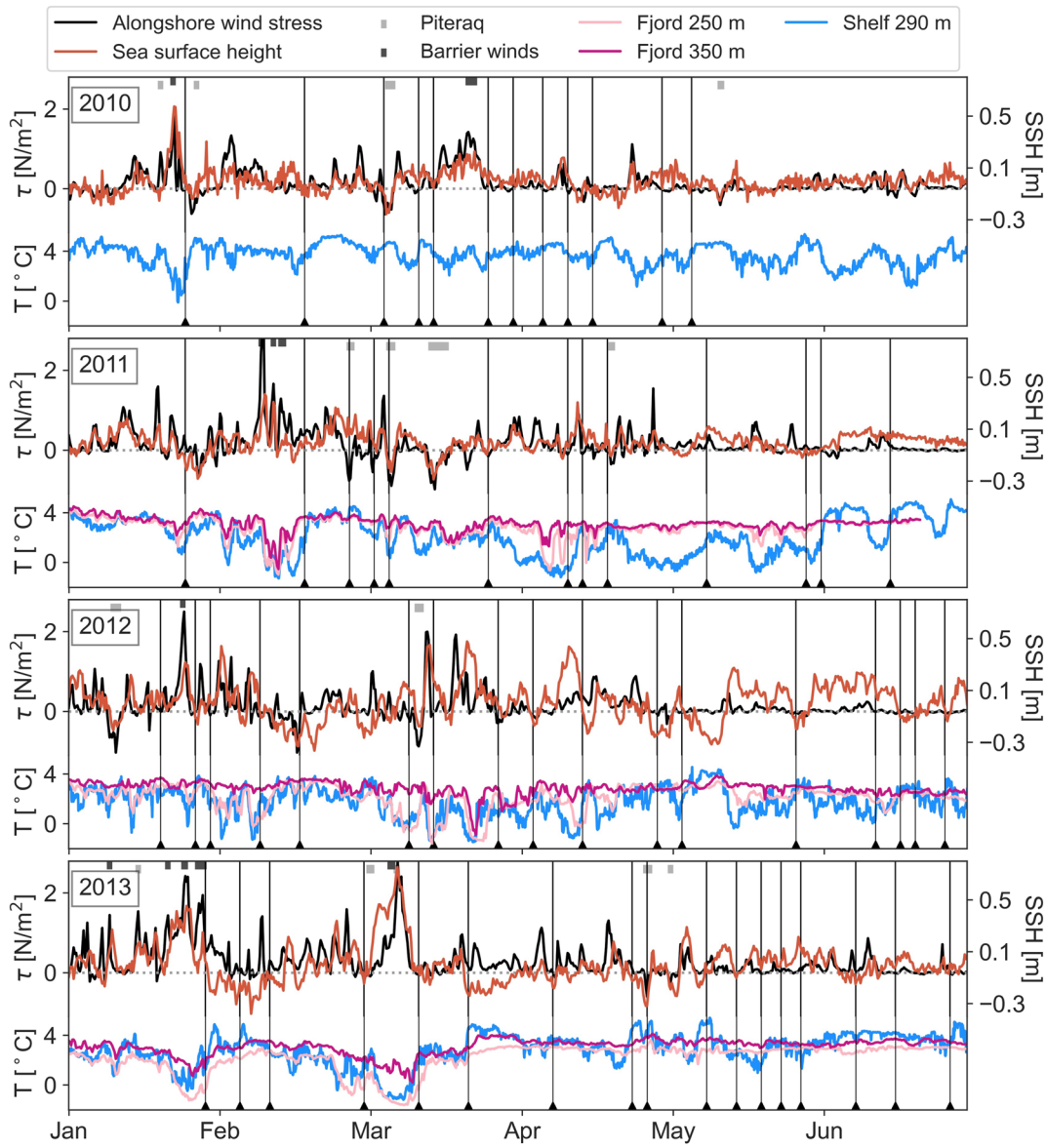

Figure 5. Timing of MODerate Resolution Imaging Spectroradiometer (MODIS)-identified Atlantic Water intrusion events (vertical black lines) with alongshore wind stress (black lines; positive is northeasterly), continental shelf sea surface height (SSH; orange lines), mooring ocean temperature from the continental shelf at 290 m depth (blue), and mooring ocean temperature from within the fjord at 250 m (light pink) and 350 m (dark pink) depth. Piteraq and barrier wind events are highlighted with light and dark gray bars, respectively, near the top of each panel.

northeasterly winds (typically >10 m/s; Figure 5); the latter occurred less frequently (19%). For the events that occurred when winds came from a westerly direction, the duration of those winds was between 6 and 90 hr. Intrusions often (78%) coincided with a SSH drop (mean change between the 18 hr before and after the intrusion began: 10 ± 2 cm). Only one intrusion occurred with persistent, weak northeasterly winds (i.e., unfavorable downwelling conditions), although the event coincided with a cyclone passing over the Irminger Sea.

3.3. Nearshore and Fjord Ocean Temperatures

Records from atmospheric reanalysis products and ocean moorings show that alongshore wind stresses have significant ($p < 0.05$) positive correlations with SSH and negative correlations with inshore ocean warming (Figure S2 in Supporting Information S1). We also created normalized composites of atmospheric and ocean

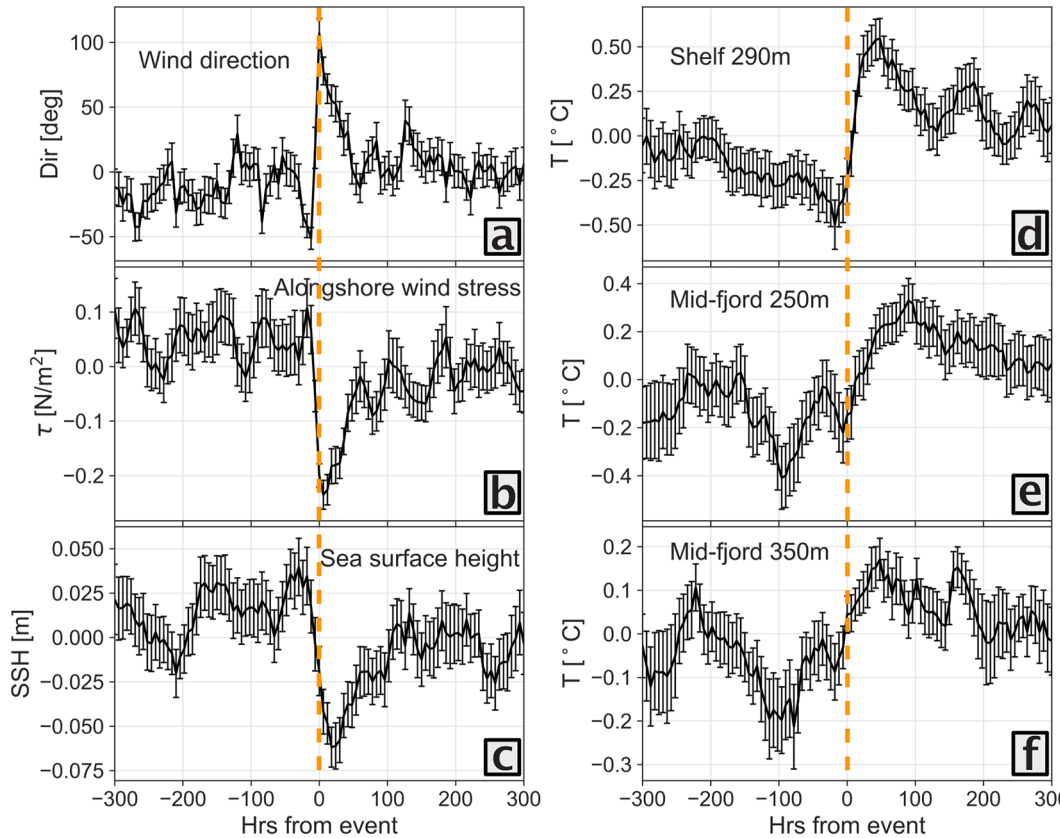

Figure 6. Composites of atmospheric and ocean parameters during the 58 visually identified AW intrusion events: (a) ERA-5 wind direction, (b) alongshore wind stress (positive means northeasterly), (b) sea surface height (SSH), and mooring temperatures from (d) the continental shelf near Sermilik Fjord mouth (290 m) and midfjord at (e) 250 m and (f) 350 m depth. Orange lines indicate the onset of negative alongshore wind forcing, and hours are the same as in (a). Error bars indicate the standard error of the mean across the events. We note that the standard deviation representing the dispersion of the data around the mean is 7.6 times larger than the shown standard error.

variability during intrusion events (Figure 6) to help distinguish between lateral warm water advection into the fjord during the intrusion events and isopycnal heaving as winds shift from downwelling-to upwelling-favorable conditions. If isopycnal heaving drives the warming during upwelling, we would expect the warming to be short-lived and to see no measurable warming in the composite records once downwelling-favorable conditions set in. Alternatively, we can attribute ocean warming to advection if significant warming persisted once downwelling has occurred.

Together, the satellite thermal imagery (Figure 3) and mooring observations (Figure 6) show a shift to warmer ocean temperatures on the shelf and in the fjord during the onset of the intrusions, with the new conditions persisting for at least 8 days post-intrusion event (Figure 6). MODIS sea surface temperatures revealed surface water temperatures (Figure 3, Figure S1 in Supporting Information S1, Movie S1) within the intrusion up to ~4°C warmer than those in the EGCC and fjord, similar to AW temperatures within the IC. Further, we examined mean mooring temperature differences from the 4 days before and the 4 days after the events ($\Delta T_{4,-4}$) as an indication of temperature change (Figure 7a): the intrusion events corresponded to significant warming ($p < 0.05$) at the continental shelf mooring (0.6 ± 0.13°C) and midfjord moorings at 125 m (0.17 ± 0.10°C), 250 m (0.35 ± 0.11°C), 350 m (0.2 ± 0.07°C), and 400 m (0.07 ± 0.05°C). The mean warming trend held for $\Delta T_{4:8,-4:-8}$ (difference between mean ocean temperatures 4–8 days before and 4–8 days after the wind events) only at moorings between 250 and 350 m depth (shelf: 0.33 ± 0.18°C; midfjord 250 m: 0.28 ± 0.17°C; midfjord 350 m: 0.15 ± 0.08°C), with a maximum increase of 2–3°C during an event at those moorings (Figure 7b). These results indicate that the intrusion events led to sustained warming in the upper AW layer on the continental shelf and in the fjord (250–350 m deep; Figure 7) through laterally transporting warm AW from offshore to the continental shelf and fjord, rather than merely producing the vertical heaving of isopycnals (Jackson et al., 2014).

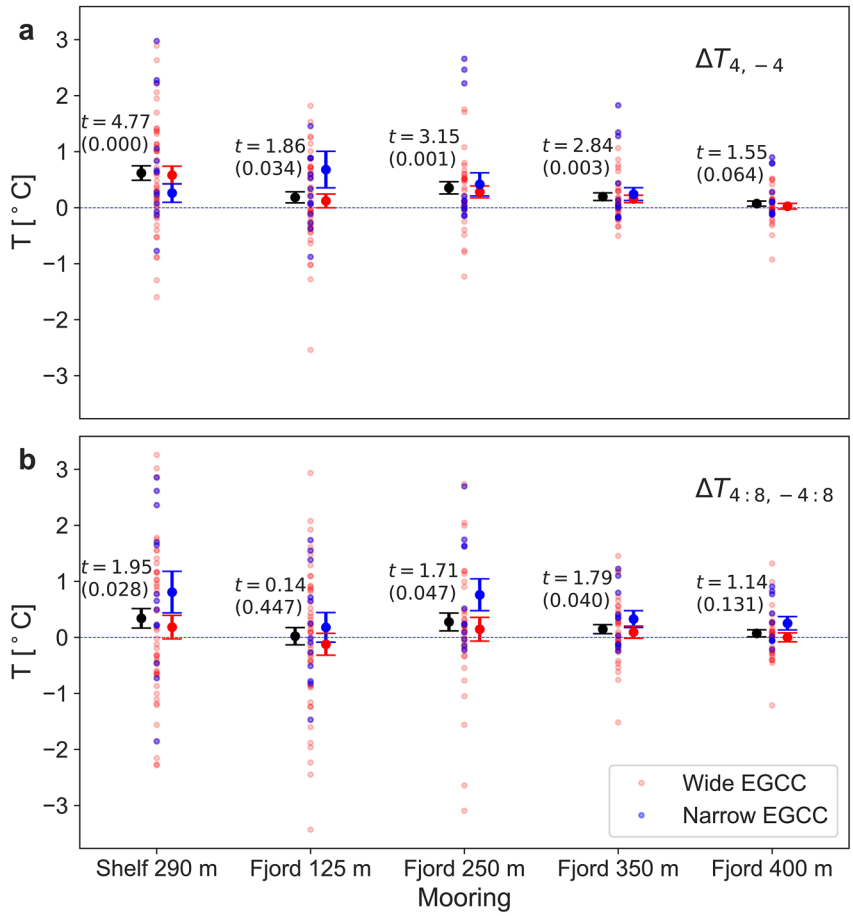

Figure 7. Mooring temperature differences averaged over (a) 4 days before and 4 days after ($\Delta T_{4,-4}$) and (b) 4–8 days before and 4–8 days after ($\Delta T_{4:8,-4:8}$) the wind events. The means of all intrusions (black) and of only the intrusions when the East Greenland Coastal Current (EGCC) was narrow (<61 km; blue) and wide (>61 km; red) are shown with 1-standard error (bars; 68% confidence interval) for each mooring location and depth. The one-sample t statistic and p value test the null hypothesis that the mean for all intrusions (black) equals 0 with the alternative hypothesis that the mean is >0.

3.4. EGCC Width

Sustained ocean warming occurred frequently (shelf: 77%, midfjord 250 m: 62%, midfjord 350 m: 54%) when the EGCC was narrow (<61 ± 14 km) and less frequently (shelf: 46%, midfjord 250 m: 46%, midfjord 350 m: 37%) when the EGCC was wider. We also observed enhanced temperature variability at the subsurface shelf mooring when the EGCC was wider ($r^2 = 0.40$; Figure S3 in Supporting Information S1), which is consistent with greater transport within the EGCC (Harden et al., 2014; Jackson et al., 2014).

4. Discussion

4.1. Reliable Detection of Intrusion Events Using MODIS Optical and Thermal Imagery

We present a unique, high temporal-resolution MODIS optical and thermal data set that, for the first time, directly captures the spatially contiguous pattern of cross-shelf upwelling flows along a continental shelf trough and provides a new method for investigating this type of flow around Greenland (and potentially elsewhere) when conditions allow (Figure 3, Figure S2 in Supporting Information S1, Movie S1). The large winter and springtime difference between PW and AW in temperature (~4°C) and sea ice extent (i.e., presence versus absence) make it possible for satellites to detect the surface variability in these water masses. Therefore, satellite imagery is particularly useful for detecting, analyzing, and quantifying the pronounced surface intrusion that cross-cuts the EGCC toward Sermilik Fjord within Sermilik Trough. These observations serve to compliment

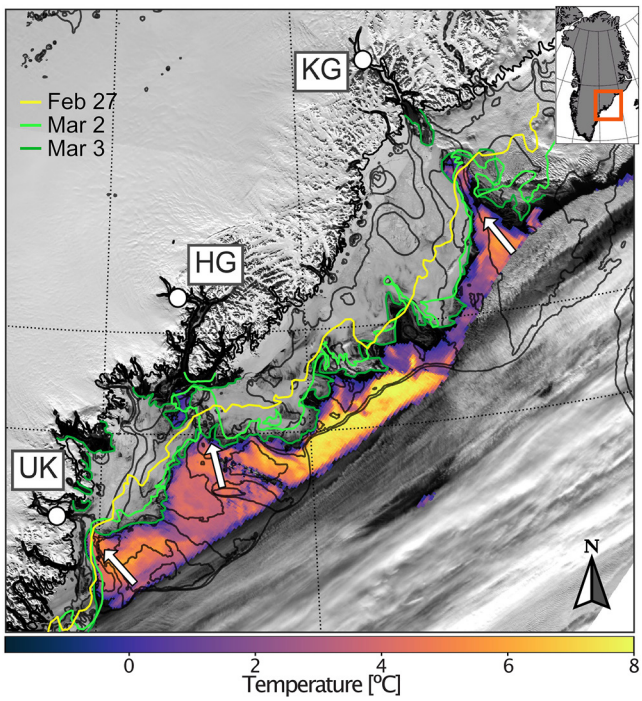

Figure 8. Coincident onshore intrusion events at multiple troughs along the southeastern Greenland continental shelf. MODerate Resolution Imaging Spectroradiometer (MODIS)-derived SST (colorscale) captures coincident AW intrusion events along the troughs leading to the three labeled glaciers: Umiiviip Kangertiva (UK), Helheim (HG), and Kangerdlugssuaq (KG) glaciers. The background imagery is from MODIS visible and thermal infrared on 2 March 2013. Hand-drawn open water edges are shown for 27 February 2013 (yellow), 1 March 2013 (light green), and 2 March 2013 (dark green). White arrows indicate troughs with intrusions and inset provides location of area in Greenland (orange).

conductivity-temperature-depth profiling (temporally limited) and mooring time series (spatially limited) to provide the surface evolution of intrusion events with high spatial and temporal coverage. This remote-sensing technique will translate well to trough systems with substantial temperature or sea ice gradients, such as other troughs along southeastern Greenland (e.g., Kangerdlugssuaq and Umiiviip Kangertiva; Figure 8).

Some limitations exist for detecting these intrusions using satellite imagery. Satellite identification of the intrusions restrict observations to AW intrusions that have surface expressions; therefore, intrusions that do not fully penetrate to the surface are not captured (or considered in this study). Further, cloud cover frequently obscures observations of the ocean surface. Thus, observations made by this method and our observations in this study likely include only a fraction of the total intrusion events during the study period. However, the available data sets support a clear characterization of the intrusion processes.

4.2. Continental Shelf and Fjord Ocean Warming

We found that AW intrusion events produced significant inshore surface and subsurface warming indicating enhanced upwelling and shoreward transport of AW along Sermilik Trough. MODIS thermal infrared imagery detected surface waters that become 4°C warmer nearshore along the Sermilik Trough during intrusion events. As captured by mooring data (Figure 6), the intrusions, on average, led to sustained warming on the continental shelf (e.g., at 290 m: 0.33 ± 0.18°C) and at some subsurface sites in the midfjord (e.g., at 250 m: 0.28 ± 0.17°C; at 350 m: 0.15 ± 0.08°C). Subsurface warming at the fjord mouth and midfjord are consistent with our satellite-based findings that the intrusions drive warm surface water inshore toward Sermilik Fjord. The subsurface warming within the fjord shows that this water is also transported into the fjord at depths between 250 and 350 m and potentially the entire AW layer in the fjord as an intrusion event progresses. These rapid events can increase subsurface AW temperatures flowing toward Helheim Glacier by as much as 2–3°C (Figure 5) and therefore present a potentially important heat transport mechanism.

4.3. Continental Shelf Circulation During Intrusion Events

Combining MODIS imagery with data from ocean moorings and atmospheric reanalysis products, we provide new insight on the dynamics of AW intrusion events linking wind-driven processes in the fjord and those on the neighboring continental shelf (Figures 1b and 1c). As observed by MODIS imagery and inferred from mooring ocean temperature records, when prevailing downwelling-favorable winds transition to upwelling-favorable winds (Figure 1c), they produce AW upwelling and a rapid (~0.2 m/s) surface and subsurface AW inflow along the Sermilik Trough. This inflow develops over only a few hours. The velocity of inflowing water is consistent with similar onshore intruding flows observed around the world (Cottier et al., 2007; Harden et al., 2014; Inall et al., 2015; Lentz et al., 2014). The onshore intrusion flow in the trough during this upwelling regime opposes surface offshore flow outside the trough. However, an opposing flow response in the trough is not manifested when winds are in the opposite direction in the downwelling regime (Figures 3, 4 and Figure S2 in Supporting Information S1). That is, the flow responses in the trough to along-shelf winds of opposite directions are asymmetric.

The intrusions in Sermilik Trough are mostly driven by cyclones and less frequently by anticyclones. Barrier wind events, which are commonly associated with the passage of cyclones through the Denmark Strait also caused intrusions. Other factors such as tides and cyclonic eddies propagating along the continental slope (Brearley et al., 2012; Bruce, 1995; Magaldi et al., 2011) may moderate intrusions, but we rule them out as primary forcing

factors because of the frequency mismatch (tides and eddies: superinertial to 1–2 days; intrusions: >2 days). Meanwhile, coincident onshore intrusions can occur over a Greenland coastal region much larger than a mesoscale eddy (Figure 8; Bruce, 1995). We also rule out piteraqs, which rarely coincide with AW intrusions (12%; Table S1), although piteraqs may contribute to fjord surface outflow and potentially subsurface outflow (Spall et al., 2017) when they cooccur with upwelling-favorable winds on the continental shelf.

Our observations of the appearance of warm water at the surface (upwelling and inflow) and at depth (warming from inflow at depth) in Sermilik Trough, as well as the timing of these events (<1 day lag with upwelling-favorable winds) are consistent with bathymetrically induced onshore intrusion of warm AW. The observed AW onshore intrusion along the Sermilik Trough's northeastern flank is consistent with localized upwelling flow on the upstream (in the sense of CTW propagation) slope of a continental shelf/slope canyon (Allen & Hickey, 2010; She & Klinck, 2000; Zhang & Lentz, 2017). This interpretation is also supported by previous work showing that ocean densities along the onshore side of Sermilik Trough (the northwestern flank) correlate more closely with wind forcing than those on the offshore side (Harden et al., 2014). Therefore, during upwelling-favorable winds or a sudden reduction in downwelling-favorable winds, water along the trough's northeastern flank likely upwells and flows shoreward throughout the water column, lifting dense AW from the continental slope toward Sermilik Fjord (Figure 1b).

Our proposed process of localized upwelling driving intrusion events is consistent with previous studies showing onshore flows in continental shelf/slope canyons associated with arrested (i.e., standing) CTWs (Kämpf, 2007; Lentz et al., 2014; She & Klinck, 2000; Zhang & Lentz, 2017). The onshore flow of the intrusion at the trough is likely either a part of a standing CTW that is excited at the trough with a southwestward propagation tendency and then arrested by a sustained northeastward shelf flow, or a transient consequence of the excessive onshore pressure gradient force during a rapid reduction of the southwestward shelf flow. We term it an "excessive" onshore pressure gradient force because it exceeds the pressure gradient force required for the cross-shelf geostrophic balance. This excessive force is caused by the greater water depth in the trough breaking the cross-shelf geostrophic balance (with cross-shelf sea level tilt) achieved over the shallower depth outside of the trough (Allen & Hickey, 2010). In both scenarios, the canyon flow is ageostrophic with an $\mathcal{O}(1)$ Rossby number, where Rossby number $Ro = U/(fL)$ (Hampson, 2020; Lentz et al., 2014; Zhang & Lentz, 2017). Here, U is a scale of the along-shelf flow, f is the Coriolis parameter, and L is a length scale of the canyon/trough. Both the observed asymmetric responses of the trough flow under coastal upwelling versus downwelling and the intensification of onshore flow along the right (northeastern) side of Sermilik Trough match the modeled surface expression of arrested CTWs over a canyon (Zhang & Lentz, 2017).

Since the Ro of the intrusion flow in Sermilik Trough is $\mathcal{O}(1)$, we hypothesize that the observed onshore intrusions in Sermilik Trough resulted from CTWs that were excited and arrested at the trough and represent an asymmetric response of the trough circulation to ambient along-shelf flows of opposite directions. During downwelling-favorable winds, enhancement of the offshore flow in a trough is minimal (Allen & Madron, 2009; Lentz et al., 2014) as topographically generated CTWs propagate freely downstream (to the southwest in this case) away from the trough. Therefore, downwelling-favorable and upwelling-favorable winds do not drive equivalent opposing flows along the trough, and oscillatory along-shelf winds can generate localized net onshore inflow in the trough, which is apparent in the MODIS imagery (Figure 3).

The localized intrusion transports offshore warm water toward the fjord and alters water properties along the way (Håvik & Våge, 2018). This impact is undiminished during the subsequent return of the winds to downwelling-favorable (Figures 6d and 6f) and thus cumulative. For this reason, even if the intruding AW is not advected into the fjord immediately during an upwelling event, the AW brought onto the shelf can be delivered into the fjord and enhance warming there during subsequent upwelling events (Fraser et al., 2018; Kämpf, 2006). During weak wind periods, the oscillatory shelf flows are also weak with a low Ro (Kämpf, 2009; Lentz et al., 2014) and would not produce net onshore intrusion of the offshore warm AW. This process could explain why only some wind-driven intermediary circulation within Sermilik Fjord results in advection of warm waters into the fjord (Jackson et al., 2014, 2018).

Although our findings qualitatively agree with modeling studies of arrested-CTW-induced onshore flows in canyons, differences in the flows may exist. In particular, previous studies (e.g., Hampson, 2020; Zhang & Lentz, 2017) used relatively simple coastlines and bathymetries, which are not representative of the complex study area. The Sermilik system has a bending coastline and a trough carved into an undulating continental shelf

that leads to a fjord. Moreover, during upwelling-favorable winds, the EGCC does not necessarily reverse, but may merely slow down at times (Foukal et al., 2020; Sutherland & Pickart, 2008). This difference suggests that at times there could be no northeastward shelf flow to arrest CTWs. In the case that the flow reversal did not occur, the intrusions may be a transient response of the trough flow to a sudden weakening of the EGCC: onshore intrusion flow could result from an excessive onshore pressure gradient induced by the cross-shelf sea level tilt over the deep trough. However, the timescale associated with this process remains unknown. To understand the details of the onshore intrusion flow and confirm its formation mechanism, further modeling work of the Sermilik circulation system is needed.

4.4. A Driver of Fjord Circulation

Our observations suggest that after the onset of the onshore intrusion, AW flowed into Sermilik Fjord toward Helheim Glacier, resulting from concurrent wind-driven intermediary circulation within the fjord (Figure 1c). During an intrusion event, we observed in imagery a large surface outflow (~0.35–0.7 m/s) from the fjord, which is presumably coincident with AW inflow at depth based on the physics of wind-driven intermediary circulation in Sermilik Fjord (Jackson et al., 2014; Straneo et al., 2010). The subsurface warming at multiple depths within the fjord ($\Delta T_{4:8,-4:8} = 0.28 \pm 0.17$°C at 250 m; $\Delta T_{4:8,-4:8} = 0.15 \pm 0.08$°C at 350 m) supports this interpretation. Sustained subsurface warming likely stems from a combination of the following during intermediary current reversals within the fjord: (a) subsurface influx into the fjord of offshore-derived AW that directly stems from the intrusion, and (b) mixing of subsurface AW within the water column during velocity reversals. Glacier-meltwater-driven circulation is weak in wintertime (Sciascia et al., 2014; Straneo et al., 2010) and relatively weak in comparison to the MODIS-observed flooding of surface water out of the fjord; therefore, we conclude that the meltwater has a minimal contribution to the dynamics.

4.5. Intrusion Suppression by the EGCC

The EGCC likely serves as a barrier to the wind-driven AW intrusions by increasing the physical distance that AW must travel to reach Sermilik Fjord (Murray et al., 2010). Our results indicate that warming occurred on the continental shelf over 77% of the time when the EGCC was narrow, substantially more common than when the EGCC was wide (55% of the time; Figure 7). Narrowing of the EGCC allows a more efficient AW intrusion onto the shelf by reducing the distance AW must travel to reach the fjord and the extent to which the water dilutes along the way (Snow et al., 2021).

Enhanced ambient continental shelf stratification and greater sea ice concentrations caused by the EGCC may also suppress inshore intrusion flow in the *surface* layer. Consistent with enhanced temperature variability observed at the subsurface shelf mooring ($r^2 = 0.40$; Figure S3 in Supporting Information S1), a seasonal widening of the EGCC coincides with EGCC greater transport (Harden et al., 2014) and increased stratification of the deeper water layers along the inner shelf (Harden et al., 2014; Jackson et al., 2014). Modeling studies have suggested that strong stratification can create a lid over upwelling within a canyon and cause isopycnals to squeeze together between the base of the surface layer and the rim of the canyon (Ramos-Musalem & Allen, 2019). That is, a deeper pycnocline suppresses the vertical extent of the bathymetry's influence and thus reduces the chance of upwelling flow reaching the surface. This vertical suppression of the intrusion would limit our ability to observe the intrusion from space and restrict the depth range in which AW is transported toward the fjord. Further, because the EGCC is often choked with sea ice in wintertime, a wide wintertime EGCC often results in greater sea ice coverage over the trough. Such conditions would decouple wind and surface ocean stresses (Martin et al., 2014) and reduce the intrusion event or prevent it from occurring. Meanwhile, we stress that, although a stronger EGCC likely suppresses intrusion events, the lack of a surface expression does not preclude the intrusion events from still occurring at depth (Figure 1c).

Together, wind characteristics (duration and magnitude) and EGCC width likely regulate when the wind events can effectively transport AW across the continental shelf and into Sermilik Fjord. Modeling of a simple canyon system suggest that intrusions resulting from upwelling-favorable winds intensify throughout the first 24 hr and remain at that strength as long as the winds persist (Zhang & Lentz, 2017). This result suggests that the strength and duration of an upwelling alongshore wind event could greatly affect overall AW transport during an upwelling event. Further, when the EGCC widens and deepens, greater wind forcing is likely required to

produce intrusions and enhanced heat transport. Vertical turbulence during upwelling tends to diffuse stratification (Ramos-Musalem & Allen, 2019), making the intrusion more likely to extend upwards in the water column with time. Offshore AW temperature and its vertical distribution also may moderate whether warming or cooling is observed inshore and within the fjord (Fraser et al., 2018). Other factors that may impact the recorded warming signals inshore include source water temperature variability—potentially linked with EGCC width (Figure S1b in Supporting Information S1)—or a rapid subsequent temperature fluctuation. For instance, a coastal downwelling occurring 4–8 days after an intrusion would be considered by our analysis as a cooling event (Figure S1c in Supporting Information S1).

5. Summary and Outlook

Satellite-derived visible and thermal imagery have tremendous potential for detecting local to regional ocean circulation processes across the globe. Using this new satellite-based observational record of intrusion events along Sermilik Trough in conjunction with wind reanalysis data and in situ ocean measurements has allowed us to create more temporally and spatially holistic observations of intrusion events than has been previously achieved in studies of similar oceanic events around the world. With this data set, we document the existence of the intrusion events, which are caused by an asymmetrical response of trough flows to opposing winds and drive onshore intrusion of warm offshore (AW) water toward Sermilik Fjord in southeast Greenland. These intrusions can substantially impact heat transport toward Sermilik Fjord and Helheim Glacier and likely other large glacier systems around Greenland. These findings provide insight into entire continental shelf circulation that are nearly impossible to capture with field-based measurements alone, helping us to fill in gaps in current knowledge of the processes that connect the broader ocean to southeast Greenland fjords.

With this broader view of the southeast Greenland continental shelf, we have identified important atmospheric and ocean feedbacks that may moderate ocean heat transport toward southeast Greenland glaciers. If more frequent upwelling-favorable wind events were to occur, this shift would lead to higher volumes of AW (and its heat) flushing onto the shelf and into Sermilik Fjord. Greater cyclone and barrier wind activity, specific high pressure blocking patterns and a high NAO index (which relates to storm variability in southeastern Greenland; Harden et al., 2011; Straneo & Heimbach, 2013) could all increase intrusion frequency based on our results. Further, EGCC weakening as a result of reduced freshwater and sea ice transport out of the Arctic (Harden et al., 2014), enhanced PW ejection off the continental shelf, and reduced Greenland Ice Sheet runoff/iceberg calving (Sutherland & Pickart, 2008) will permit more intrusion events, reduce the AW dilution as it crosses the continental shelf, and make southeast Greenland fjords more susceptible to warm water intrusion (Murray et al., 2010; Snow et al., 2021). These intrusion events can result in 2–3°C of warming in the fjord, and models may be able to predict years of high onshore heat transport using this improved understanding of the linkage between subsurface water temperatures, EGCC width and transport, and intrusion-favorable winds. A better understanding of the deep-water onshore transport processes that may directly feed into Sermilik Fjord and bring heat to Helheim Glacier has substantial implications for pinpointing the role of the ocean in glacier change in the past and future. Intrusion events of this nature may also occur to varying extents at other glacier systems around Greenland, such as Kangerdlugssuaq Glacier (Fraser et al., 2018), which could make it an important mechanism for regulating the mass loss of a large-scale ice sheet.

Data Availability Statement

Processed data used in Table S1 (xlsx) are permanently archived at the Arctic Data Center (https://doi.org/10.18739/A2959C90P; Snow, 2023a) and all data used in the production of this manuscript are available with the Python Jupyter Notebook processing and analysis code on Zenodo (https://github.com/tsnow03/AtlanticWaterIntrusions2023; https://doi.org/10.5281/zenodo.8335192; Snow, 2023b). Users of the code should contact the author to ensure reasonable applications of the method. The mooring data used in this paper are available at the National Oceanographic Data Center (https://data.nodc.noaa.gov/cgi-bin/iso?id=gov.noaa.nodc:0123282, 0126772, 0127320, and 0127325). Sea surface height data were provided by B. Harden and are available with the Jupyter Notebook. Sea surface temperature-derived EGCC widths were extracted from data archived at the Arctic Data Center (https://doi.org/10.18739/A2348GH20; Snow et al., 2020). Programme for Monitoring of the Greenland Ice Sheet MIT weather station wind fields can be found at https://doi.org/10.22008/FK2/IW73UU. Level 2 MODIS visible and thermal infrared imagery can be found at search.earthdata.nasa.gov (MOD/MYD09:

https://doi.org/10.5067/MODIS/MOD09.006 and https://doi.org/10.5067/MODIS/MYD09.006, GHRSST: https://doi.org/10.5067/GHMDA-2PJ02 and https://doi.org/10.5067/GHMDA-2PJ19). ECMWF ERA-5 ensemble (EDA) subdaily nonwave (enda) analysis (an) data are located at https://apps.ecmwf.int/data-catalogues/era5/?type=an&class=ea&stream=enda&expver=1.

Acknowledgments
We gratefully acknowledge the National Aeronautics and Space Administration (NASA), the U.S. National Science Foundation (NSF), and the Cooperative Institute for Research in Environmental Sciences (CIRES). This work was supported by NASA Headquarters under a NASA Earth and Space Science Fellowship Program—Grant (NNX16AO33H) and the NASA Cryosphere (80NSSC22K0385, 80NSSC22K1877) and Transform to Open Science Programs (80NSSC23K0002). This material is also based upon work supported by the NSF Graduate Research Fellowship Program under Grant DGE1650115. Any opinions, findings, and conclusions or recommendations expressed in this material are those of the authors and do not necessarily reflect the views of the NSF. We also acknowledge the NASA CryoCloud (Snow et al., 2023) and NSF Earth Cube Jupyter Meets the Earth projects for providing JupyterHub cloud-computing platforms where some of this research was conducted. We thank Kathleen Bogan (CIRES) for her artistic design of Figures 1b and 1c. We also thank our reviewers and editor for their comments that greatly improved the quality of this paper.

References

Allen, S. E., & de Madron, X. D. (2009). A review of the role of submarine canyons in deep-ocean exchange with the shelf. *Ocean Science*, *5*(4), 607–620. https://doi.org/10.5194/os-5-607-2009

Allen, S. E., & Hickey, B. M. (2010). Dynamics of advection-driven upwelling over a shelf break submarine canyon. *Journal of Geophysical Research*, *115*, C08018. https://doi.org/10.1029/2009JC005731

Bjørk, A. A., Kjær, K. H., Korsgaard, N. J., Khan, S. A., Kjeldsen, K. K., Andresen, C. S., et al. (2012). An aerial view of 80 years of climate-related glacier fluctuations in southeast Greenland. *Nature Geoscience*, *5*(6), 427–432. https://doi.org/10.1038/ngeo1481

Brearley, J. A., Pickart, R. S., Valdimarsson, H., Jonsson, S., Schmitt, R. W., & Haine, T. W. N. (2012). The East Greenland boundary current system south of Denmark Strait. *Deep Sea Research Part I: Oceanographic Research Papers*, *63*, 1–19. https://doi.org/10.1016/j.dsr.2012.01.001

Bruce, J. G. (1995). Eddies southwest of the Denmark strait. *Deep Sea Research Part I: Oceanographic Research Papers*, *42*(1), 13–29. https://doi.org/10.1016/0967-0637(94)00040-y

Copernicus Climate Change Service. (2017). ERA5: Fifth generation of ECMWF atmospheric reanalyses of the global climate [Dataset]. Retrieved from https://cds.climate.copernicus.eu

Cottier, F., Nilsen, F., Inall, M. E., Gerland, S., Tverberg, V., & Svendsen, H. (2007). Wintertime warming of an Arctic shelf in response to large-scale atmospheric circulation. *Geophysical Research Letters*, *34*, L10607. https://doi.org/10.1029/2007GL029948

Cottier, F., Tverberg, V., Inall, M., Svendsen, H., Nilsen, F., & Griffiths, C. (2005). Water mass modification in an Arctic fjord through cross-shelf exchange: The seasonal hydrography of Kongsfjorden, Svalbard. *Journal of Geophysical Research*, *110*, C12005. https://doi.org/10.1029/2004JC002757

Cowton, T., Sole, A., Nienow, P., Slater, D., & Hanna, E. (2016). Controls on the transport of oceanic heat to Kangerdlugssuaq Glacier, east Greenland. *Journal of Glaciology*, *62*(236), 1167–1180. https://doi.org/10.1017/jog.2016.117

Crawford, A. D., Alley, K. E., Cooke, A. M., & Serreze, M. C. (2020). Synoptic climatology of rain-on-snow events in Alaska synoptic climatology of rain-on-snow events in Alaska. *Monthly Weather Review*, *148*(3), 1275–1295. https://doi.org/10.1175/mwr-d-19-0311.1

Crawford, A. D., & Serreze, M. C. (2016). Does the summer Arctic frontal zone influence Arctic ocean cyclone activity? *Journal of Climate*, *29*(13), 4977–4993. https://doi.org/10.1175/JCLI-D-15-0755.1

Foukal, N. P., Gelderloos, R., & Pickart, R. S. (2020). A continuous pathway for fresh water along the East Greenland shelf. *Science Advances*, *6*(43), eabc4254. https://doi.org/10.1126/sciadv.abc4254

Fraser, N. J., & Inall, M. E. (2018). Influence of barrier wind forcing on heat delivery toward the Greenland ice sheet. *Journal of Geophysical Research: Oceans*, *123*, 2513–2538. https://doi.org/10.1002/2017JC013464

Fraser, N. J., Inall, M. E., Magaldi, M. G., Haine, T. W. N., & Jones, S. C. (2018). Wintertime fjord-shelf interaction and ice sheet melting in southeastsoutheast Greenland. *Journal of Geophysical Research: Oceans*, *123*, 9156–9177. https://doi.org/10.1029/2018JC014435

Gelderloos, R., Haine, T. W. N., & Almansi, M. (2021). Coastal trapped waves and other Subinertial variability along the southeastsoutheast Greenland coast in a Realistic Numerical Simulation. *Journal of Physical Oceanography*, *51*(3), 861–877. https://doi.org/10.1175/JPO-D-20-0239.1

Hampson, P. (2020). *Glacial troughs eject wind-driven shelf circulation to the slope (Unpublished master's thesis)*. University of New Hampshire. Retrieved from https://scholars.unh.edu/thesis/1343

Harden, B. E., Renfrew, I. A., & Petersen, G. N. (2011). A climatology of wintertime barrier winds off southeast Greenland. *Journal of Climate*, *24*(17), 4701–4717. https://doi.org/10.1175/2011JCLI4113.1

Harden, B. E., Straneo, F., & Sutherland, D. A. (2014). Moored observations of synoptic and seasonal variability in the East Greenland Coastal Current. *Journal of Geophysical Research: Oceans*, *119*, 8838–8857. https://doi.org/10.1002/2014JC010134

Håvik, L., & Våge, K. (2018). Wind-driven coastal upwelling and downwelling in the Shelfbreak east Greenland current. *Journal of Geophysical Research: Oceans*, *123*, 6106–6115. https://doi.org/10.1029/2018JC014273

Hersbach, H., Bell, B., Berrisford, P., Biavati, G., Horányi, A., Muñoz Sabater, J., et al. (2018). ERA5 hourly data on single levels from 1959 to present [Dataset]. Copernicus Climate Change Service (C3S) Climate Data Store (CDS). https://doi.org/10.24381/cds.adbb2d47

Holland, D. M., Thomas, R. H., Young, B. d., Ribergaard, M. H., & Lyberth, B. (2008). Acceleration of Jakobshavn Isbræ triggered by warm subsurface ocean waters. *Nature Geoscience*, *1*(10), 659–664. https://doi.org/10.1038/ngeo316

Howat, I. M., Joughin, I., Fahnestock, M., Smith, B., & Scambos, T. (2008). Synchronous retreat and acceleration of southeast Greenland outlet glaciers 2000–06: Ice dynamics and coupling to climate. *Journal of Glaciology*, *54*(187), 646–660. https://doi.org/10.3189/002214308786570908

Howat, I. M., Joughin, I., Tulaczyk, S., & Gogineni, S. (2005). Rapid retreat and acceleration of Helheim Glacier, east Greenland. *Geophysical Research Letters*, *32*, L22502. https://doi.org/10.1029/2005GL024737

Inall, M. E., Nilsen, F., Cottier, F. R., & Daae, R. (2015). Shelf/fjord exchange driven by coastal-trapped waves in the Arctic. *Journal of Geophysical Research: Oceans*, *120*, 8283–8303. https://doi.org/10.1002/2015JC011277

Jackson, R. H., Lentz, S. J., & Straneo, F. (2018). The dynamics of shelf forcing in Greenlandic fjords. *Journal of Physical Oceanography*, *48*(11), 2799–2827. https://doi.org/10.1175/JPO-D-18-0057.1

Jackson, R. H., & Straneo, F. (2016). Heat, salt, and freshwater budgets for a glacial fjord in Greenland. *Journal of Physical Oceanography*, *46*(9), 2735–2768. https://doi.org/10.1175/JPO-D-15-0134.1

Jackson, R. H., Straneo, F., & Sutherland, D. A. (2014). Externally forced fluctuations in ocean temperature at Greenland glaciers in non-summer months. *Nature Geoscience*, *7*(7), 503–508. https://doi.org/10.1038/ngeo2186

Johannessen, O. M., Korablev, A., Miles, V., Miles, M. W., & Solberg, K. E. (2011). Interaction between the warm subsurface atlantic water in the Sermilik fjord and Helheim Glacier in southeast Greenland. *Surveys in Geophysics*, *32*(4–5), 387–396. https://doi.org/10.1007/s10712-011-9130-6

Johnson, E. R. (1978). Quasigeostrophic flow above sloping boundaries. *Deep Sea Research*, *25*(11), 1049–1071. https://doi.org/10.1016/0146-6291(78)90586-6

JPL/OBPG/RSMAS. (2020a). *MODIS Aqua L2P swath SST data set*. PO.DAAC. Retrieved from https://doi.org/10.5067/GHMDA-2PJ19

JPL/OBPG/RSMAS. (2020b). *MODIS Terra L2P swath SST data set*. PO.DAAC. Retrieved from https://doi.org/10.5067/GHMDT-2PJ19

Kämpf, J. (2006). Transient wind-driven upwelling in a submarine canyon: A process-oriented modeling study. *Journal of Geophysical Research*, *111*, C11011. https://doi.org/10.1029/2006JC003497
Kämpf, J. (2007). On the magnitude of upwelling fluxes in shelf-break canyons. *Continental Shelf Research*, *27*(17), 2211–2223. https://doi.org/10.1016/j.csr.2007.05.010
Kämpf, J. (2009). On the interaction of time-variable flows with a Shelfbreak canyon. *Journal of Physical Oceanography*, *39*(1), 248–260. https://doi.org/10.1175/2008jpo3753.1
Kämpf, J. (2012). Lee effects of localized upwelling in a shelf-break canyon. *Continental Shelf Research*, *42*, 78–88. https://doi.org/10.1016/j.csr.2012.05.005
Killworth, P. D. (1978). Coastal upwelling and Kelvin waves with small longshore topography. *Journal of Physical Oceanography*, *8*(2), 188–205. https://doi.org/10.1175/1520-0485(1978)008<0188:CUAKWW>2.0.CO;2
Kilpatrick, K. A., Podestá, G., Walsh, S., Williams, E., Halliwell, V., Szczodrak, M., et al. (2015). A decade of sea surface temperature from MODIS. *Remote Sensing of Environment*, *165*, 27–41. https://doi.org/10.1016/j.rse.2015.04.023
Klinck, J. M. (1996). Circulation near submarine canyons: A modeling study. *Journal of Geophysical Research*, *101*(C1), 1211–1223. https://doi.org/10.1029/95JC02901
Le Bras, I., Straneo, F., Holte, J., & Holliday, P. N. (2018). Seasonality of freshwater in the East Greenland current system from 2014 to 2016. *Journal of Geophysical Research: Oceans*, *123*, 8828–8848. https://doi.org/10.1029/2018JC014511
Lentz, S. J., Butman, B., & Harris, C. (2014). The vertical structure of the circulation and dynamics in Hudson Shelf Valley. *Journal of Geophysical Research: Oceans*, *119*, 3694–3713. https://doi.org/10.1002/2014JC009883
Luckman, A., Murray, T., Lange, R. d., & Hanna, E. (2006). Rapid and synchronous ice-dynamic changes in East Greenland. *Geophysical Research Letters*, *33*, L03503. https://doi.org/10.1029/2005GL025428
Magaldi, M. G., Haine, T. W. N., & Pickart, R. S. (2011). On the nature and variability of the East Greenland Spill Jet: A case study in summer 2003. *Journal of Physical Oceanography*, *41*(12), 2307–2327. https://doi.org/10.1175/JPO-D-10-05004.1
Martin, T., Steele, M., & Zhang, J. (2014). Seasonality and long-term trend of Arctic Ocean surface stress in a model. *Journal of Geophysical Research: Oceans*, *119*, 1723–1738. https://doi.org/10.1002/2013JC009425
Millan, R., Rignot, E., Mouginot, J., Wood, M., Bjørk, A., & Morlighem, M. (2018). Vulnerability of southeast Greenland glaciers to warm Atlantic water from operation IceBridge and ocean melting Greenland data. *Geophysical Research Letters*, *45*, 2688–2696. https://doi.org/10.1002/2017GL076561
Minnett, P., Alvera-Azcárate, A., Chin, T., Corlett, G., Gentemann, C., Karagali, I., et al. (2019). Half a century of satellite remote sensing of sea-surface temperature. *Remote Sensing of Environment*, *233*, 111366. https://doi.org/10.1016/j.rse.2019.111366
MODIS Characterization Support Team. (2017). MODIS 500 m calibrated radiance product [Dataset]. https://doi.org/10.5067/MODIS/MOD02HKM.061
Moore, G. W. K., Renfrew, I. A., Harden, B. E., & Mernild, S. H. (2015). The impact of resolution on the representation of southeast Greenland barrier winds and katabatic flows. *Geophysical Research Letters*, *42*, 3011–3018. https://doi.org/10.1002/2015GL063550
Morlighem, M., Williams, C. N., Rignot, E., An, L., Arndt, J. E., Bamber, J. L., et al. (2017). BedMachine v3: Complete bed topography and ocean bathymetry mapping of Greenland from multibeam echo sounding combined with mass conservation. *Geophysical Research Letters*, *44*, 11051–11061. https://doi.org/10.1002/2017GL074954
Mouginot, J., Rignot, E., Scheuchl, B., Fenty, I., Khazendar, A., Morlighem, M., et al. (2015). Fast retreat of ZachariæIsstrøm, northeast Greenland. *Science*, *350*(6266), 1357–1361. https://doi.org/10.1126/science.aac7111
Murray, T., Scharrer, K., James, T., Dye, S., Hanna, E., Booth, A., et al. (2010). Ocean regulation hypothesis for glacier dynamics in southeast Greenland and implications for ice sheet mass changes. *Journal of Geophysical Research*, *115*. F03026. https://doi.org/10.1029/2009JF001522
Nilsen, F., Cottier, F., Skogseth, R., & Mattsson, S. (2008). Fjord–shelf exchanges controlled by ice and brine production: The interannual variation of Atlantic water in Isfjorden, Svalbard. *Continental Shelf Research*, *28*(14), 1838–1853. https://doi.org/10.1016/j.csr.2008.04.015
Oltmanns, M., Straneo, F., Moore, G., & Mernild, S. (2014). Strong downslope wind events in Ammassalik, southeast Greenland. *Journal of Climate*, *27*(3), 977–993. https://doi.org/10.1175/JCLI-D-13-00067.1
Ramos-Musalem, K., & Allen, S. E. (2019). The impact of locally-enhanced vertical diffusivity on the cross-shelf transport of tracers induced by a submarine canyon. *Journal of Physical Oceanography*, *49*(2), 561–584. https://doi.org/10.1175/JPO-D-18-0174.1
Rudels, B., Fahrbach, E., Meincke, J., Budéus, G., & Eriksson, P. (2002). The East Greenland current and its contribution to the Denmark strait overflow. *ICES Journal of Marine Science*, *59*(6), 1133–1154. https://doi.org/10.1006/jmsc.2002.1284
Sciascia, R., Cenedese, C., Nicolì, D., Heimbach, P., & Straneo, F. (2014). Impact of periodic intermediary flows on submarine melting of a Greenland glacier. *Journal of Geophysical Research: Oceans*, *119*, 7078–7098. https://doi.org/10.1002/2014JC009953
She, J., & Klinck, J. M. (2000). Flow near submarine canyons driven by constant winds. *Journal of Geophysical Research*, *105*(C12), 28671–28694. https://doi.org/10.1029/2000JC900126
Snow, T. (2023a). Sermilik Trough Atlantic Water intrusion events (2010-2013). NSF Arctic Data Center. https://doi.org/10.18739/A2959C90P
Snow, T. (2023b). tsnow03/AtlanticWaterIntrusions2023: Atlantic_Water_intrusions_2023 (Version 2023.09.11) [Computer software]. Zenodo. https://doi.org/10.5281/ZENODO.8335192
Snow, T., Abdalati, W., & Scambos, T. (2020). Sea surfaces temperatures near Sermilik Fjord and Helheim Glacier (2000-2018) [Dataset]. NSF Arctic Data Center. https://doi.org/10.18739/A2348GH20
Snow, T., Millstein, J., Scheick, J., Sauthoff, W., Leong, W. J., Colliander, J., et al. (2023). CryoCloud JupyterBook (Computational Notebook). Zenodo. https://doi.org/10.5281/zenodo.7576602
Snow, T., Straneo, F., Holte, J., Grigsby, S., Abdalati, W., & Scambos, T. (2021). More than skin deep: Sea surface temperature as a means of inferring Atlantic water variability on the southeastsoutheast Greenland continental shelf near Helheim Glacier. *Journal of Geophysical Research: Oceans*, *126*, e2020JC016509. https://doi.org/10.1029/2020JC016509
Spall, M. A., Jackson, R. H., & Straneo, F. (2017). Katabatic wind-driven exchange in fjords. *Journal of Geophysical Research: Oceans*, *122*, 8246–8262. https://doi.org/10.1002/2017JC013026
Straneo, F., Curry, R., Sutherland, D., Hamilton, G., Cenedese, C., Våge, K., & Stearns, L. A. (2011). Impact of fjord dynamics and glacial runoff on the circulation near Helheim Glacier. *Nature Geoscience*, *4*(5), 322–327. https://doi.org/10.1038/ngeo1109
Straneo, F., Hamilton, G. S., Sutherland, D. A., Stearns, L. A., Davidson, F., Hammill, M. O., et al. (2010). Rapid circulation of warm subtropical waters in a major glacial fjord in East Greenland. *Nature Geoscience*, *3*(3), 182–186. https://doi.org/10.1038/ngeo764
Straneo, F., & Heimbach, P. (2013). North Atlantic warming and the retreat of Greenland's outlet glaciers. *Nature*, *504*(7478), 36–43. https://doi.org/10.1038/nature12854
Sutherland, D. A., & Pickart, R. S. (2008). The East Greenland coastal current: Structure, variability, and forcing. *Progress in Oceanography*, *78*(1), 58–77. https://doi.org/10.1016/j.pocean.2007.09.006

Sutherland, D. A., Straneo, F., & Pickart, R. S. (2014). Characteristics and dynamics of two major Greenland glacial fjords. *Journal of Geophysical Research: Oceans*, *119*, 3767–3791. https://doi.org/10.1002/2013JC009786

Sutherland, D. A., Straneo, F., Stenson, G. B., Davidson, F., Hammill, M. O., & Rosing-Asvid, A. (2013). Atlantic water variability on the SE Greenland continental shelf and its relationship to SST and bathymetry. *Journal of Geophysical Research: Oceans*, *118*, 847–855. https://doi.org/10.1029/2012JC008354

Svendsen, H., & Thompson, R. O. R. Y. (1978). Wind-driven circulation in a fjord. *Journal of Physical Oceanography*, *8*(4), 703–712. https://doi.org/10.1175/1520-0485(1978)008<0703:WDCIAF>2.0.CO;2

Våge, K., Pickart, R. S., Sarafanov, A., Knutsen, O., Mercier, H., Lherminier, P., et al. (2011). The Irminger Gyre: Circulation, convection, and interannual variability. *Deep Sea Research Part I: Oceanographic Research Papers*, *58*(5), 590–614. https://doi.org/10.1016/j.dsr.2011.03.001

Williams, J. J., Gourmelen, N., Nienow, P., Bunce, C., & Slater, D. (2021). Helheim glacier poised for dramatic retreat. *Geophysical Research Letters*, *48*, e2021GL094546. https://doi.org/10.1029/2021GL094546

Zhang, W. G., & Lentz, S. J. (2017). Wind-driven circulation in a Shelf Valley. Part I: Mechanism of the asymmetrical response to along-shelf winds in opposite directions. *Journal of Physical Oceanography*, *47*(12), 2927–2947. https://doi.org/10.1175/JPO-D-17-0083.1